Geophysical Research Letters

RESEARCH LETTER
10.1029/2025GL117419

Induced Earthquakes in the Southern Delaware Basin, Texas, Are Bound by a Geomechanically Controlled Maximum Magnitude

James P. Verdon[1] **and Ryan Schultz**[2]

[1]School of Earth Sciences, University of Bristol, Bristol, UK, [2]Department of Earth Sciences, Swiss Seismological Service, ETH Zürich, Zürich, Switzerland

Key Points:

- Induced seismicity in the southern Delaware Basin is truncated by a maximum magnitude at approximately M 4.0
- The M_{MAX} truncation is likely to be caused by the limited width of strata-bound faults on which the seismicity occurs
- The M_{MAX} truncation has important implications for induced seismicity hazard management

Supporting Information:

Supporting Information may be found in the online version of this article.

Correspondence to:

J. P. Verdon,
James.Verdon@bristol.ac.uk

Citation:

Verdon, J. P., & Schultz, R. (2026). Induced earthquakes in the southern Delaware Basin, Texas, are bound by a geomechanically controlled maximum magnitude. *Geophysical Research Letters*, *53*, e2025GL117419. https://doi.org/10.1029/2025GL117419

Received 4 JUN 2025
Accepted 14 JAN 2026

Author Contributions:

Conceptualization: James P. Verdon
Formal analysis: James P. Verdon
Investigation: James P. Verdon
Methodology: Ryan Schultz
Software: Ryan Schultz
Writing – original draft: James P. Verdon
Writing – review & editing: Ryan Schultz

Abstract In this paper we document the first example-the southern Delaware Basin-where widespread induced triggered (as opposed to "driven") seismicity across a large area exhibits a maximum magnitude truncation. The most likely cause of this truncation is that although the shallow faults in this area are many km in length, they are structurally constrained and have limited down-dip widths, typically no more than approximately 1 km. Ruptures on faults of such limited width are not expected to attain high aspect ratios. As such, the ruptures on such faults would be limited to dimensions of roughly 1 km^2, which corresponds to magnitudes which closely match the observed M_{MAX} truncation. The M_{MAX} truncation for induced earthquakes in the southern Delaware Basin has significant implications since it implies that down-dip fault widths may play an important role in constraining the maximum magnitudes of induced events.

Plain Language Summary This study examines the largest earthquake size–the "maximum magnitude"–for earthquakes in the southern Delaware Basin, western Texas. We find that the maximum magnitude appears to be fundamentally limited to approximately M 4.0, despite the ongoing numbers of events. The most likely explanation for this phenomenon is that the faults activated by the subsurface industrial activities have limited width (the distance from top to bottom of the fault), which limits the maximum size of earthquakes that can occur. This finding has important implications, as it means that we should focus on making better observations of fault widths when assessing induced seismicity hazard at future sites.

1. Introduction

Most sequences of induced seismicity (earthquakes caused by human activities) have been observed to follow the Gutenberg and Richter (1944) (G-R hereafter) magnitude frequency distribution (van der Elst et al., 2016; Watkins et al., 2023), where the number of earthquakes, N, larger than a given magnitude M, is given by:

$$\log_{10} N = a - bM, \tag{1}$$

where a and b are constants that are fitted to the data (e.g., Aki, 1965). The G-R relationship posits a relationship between N and M whereby an ever-increasing number of events implies the expected occurrence of events with ever-increasing magnitudes.

This relationship has great significance for the management and mitigation of induced seismicity hazard, since it entails that to reduce the magnitudes of future events occurring in a given sequence, the rate at which earthquakes occur must be reduced. Typically, this is done by moderating the rate at which the industrial activity takes place (e.g., the rate at which fluids are injected), with scaling factors computed between operational rates and seismicity (e.g., Hallo et al., 2014; Shapiro et al., 2010), and rates then adjusted until the seismic hazard is reduced to an acceptable level (Clarke et al., 2019; Hill et al., 2024; Kettlety et al., 2021; Kwiatek et al., 2019; Langenbruch & Zoback, 2016).

For natural, tectonic earthquakes, the underlying deformation that drives seismicity occurs on geological time-scales. Since the timescale of potential future observations, and therefore the number of future earthquakes, can be treated as infinite, the G-R distribution must be truncated at some upper magnitude, referred to as M_{MAX} (Bommer & Verdon, 2024; Wyss, 1979). M_{MAX} for tectonic earthquakes is typically determined by the tectonic conditions and structural geology of a region, such as the lengths of the largest faults and the seismogenic thickness of the Earth's crust, or other controls on the dimensions of earthquake ruptures.

In contrast, induced seismicity is caused by subsurface perturbations introduced by humans. These perturbations have finite duration and finite spatial extent, and the number of induced events is therefore also finite in a given sequence. In such cases, the magnitudes of the largest event, as determined by the number of events, N, and the G-R relationship, may not approach any upper truncation defined by geomechanical/tectonic limits. This has in fact proved to be the case for the overwhelming majority of induced earthquake sequences, where magnitudes are observed to be as large as statistically expected based on an unbounded G-R distribution (Bommer & Verdon, 2024; Schultz, 2024; van der Elst et al., 2016).

Some exceptions to this rule have been identified, where a geomechanical limit of some kind has imposed an upper magnitude truncation on the G-R distribution (e.g., Boitz et al., 2024; Verdon et al., 2018; Zöller & Holschneider, 2016). However, to date such examples have only been identified for cases of "industrially driven" seismicity. The distinction between "driven" and "triggered" seismicity is that for driven cases, the bulk of the strain energy that is released was imparted by the industrial activity itself (Bommer & Verdon, 2024). In contrast, for triggered seismicity, the strain energy that is released is tectonic strain that has accumulated over geological time, with the industrial activity merely serving as the trigger to nucleate earthquakes that release tectonic energy (e.g., Rodríguez-Pradilla et al., 2022).

Examples of driven seismicity typically include mining-induced seismicity associated with void-space collapses (e.g., Verdon et al., 2018), and at large, mature, depleting hydrocarbon fields that are experiencing significant subsidence (e.g., Zöller & Holschneider, 2016). In such cases, the strain energy that is released accumulates predominantly due to the human activities—for example, vertical motions created by the removal of material, either solid or liquid, from the subsurface. Driven seismicity occurs with focal mechanisms that are consistent with the strain imparted by the industrial activity—for example, dip-slip motions around compacting mature hydrocarbon reservoirs (see, e.g., Figure 4 of Segall, 1989). These focal mechanisms may co-incidentally align with regional stress conditions, but they do not have to (e.g., Verdon et al., 2018).

In contrast, examples of triggered seismicity are often represented by wastewater disposal (WWD). WWD creates small pore pressure increases which act to de-clamp faults that have been stressed by tectonic forces, allowing them to release accumulated tectonic energy. Triggered earthquakes occur on faults that are well orientated for slip in the present-day stress field (Walsh & Zoback, 2016) and have focal mechanisms that are consistent therewith (McNamara et al., 2015).

For driven seismicity, a link between the scale of the industrial activity and M_{MAX} is to be expected, and such relationships have been proposed (e.g., Galis et al., 2017; McGarr, 1976, 2014; Shapiro et al., 2011). For triggered earthquakes, there is no a priori reason to expect any link between the scale of industrial activities and M_{MAX}, as the industrial process serves only to nucleate the ruptures—the size of any resulting ruptures will be determined solely by the tectonic properties of the reactivated faults. The fact that scaling relationships for M_{MAX}, such as those proposed by McGarr (2014), cannot be applied by default to triggered seismicity, is now well-established (Bommer & Verdon, 2024; McGarr & Majer, 2023).

Nevertheless, all sequences of triggered seismicity must still have a maximum possible magnitude, based on the tectonic conditions in the volume perturbed by the industrial activity, such as the dimensions and rheological properties of existing faults. It is just that, as described by van der Elst et al. (2016), most sequences have not yet generated a sufficient number of events such that no upper magnitude truncation of the G-R distribution has yet been reached. For these cases, M_{MAX} cannot be robustly quantified (Holschneider et al., 2011). However, as the numbers of induced earthquakes continues to increase in different case examples around the world, we should expect upper magnitude truncations to become more apparent.

In this paper we report on the first instance where a large-scale sequence of triggered seismicity acting across a significant area—the WWD-induced seismicity of the southern Delaware Basin in western Texas—appears to have become limited by an M_{MAX} truncation. As well as the important implications for the resulting induced seismicity hazard, by examining the geomechanical controls that have created this magnitude truncation, we can begin to understand in the general sense the factors that may control the maximum possible magnitudes for all sequences of induced seismicity.

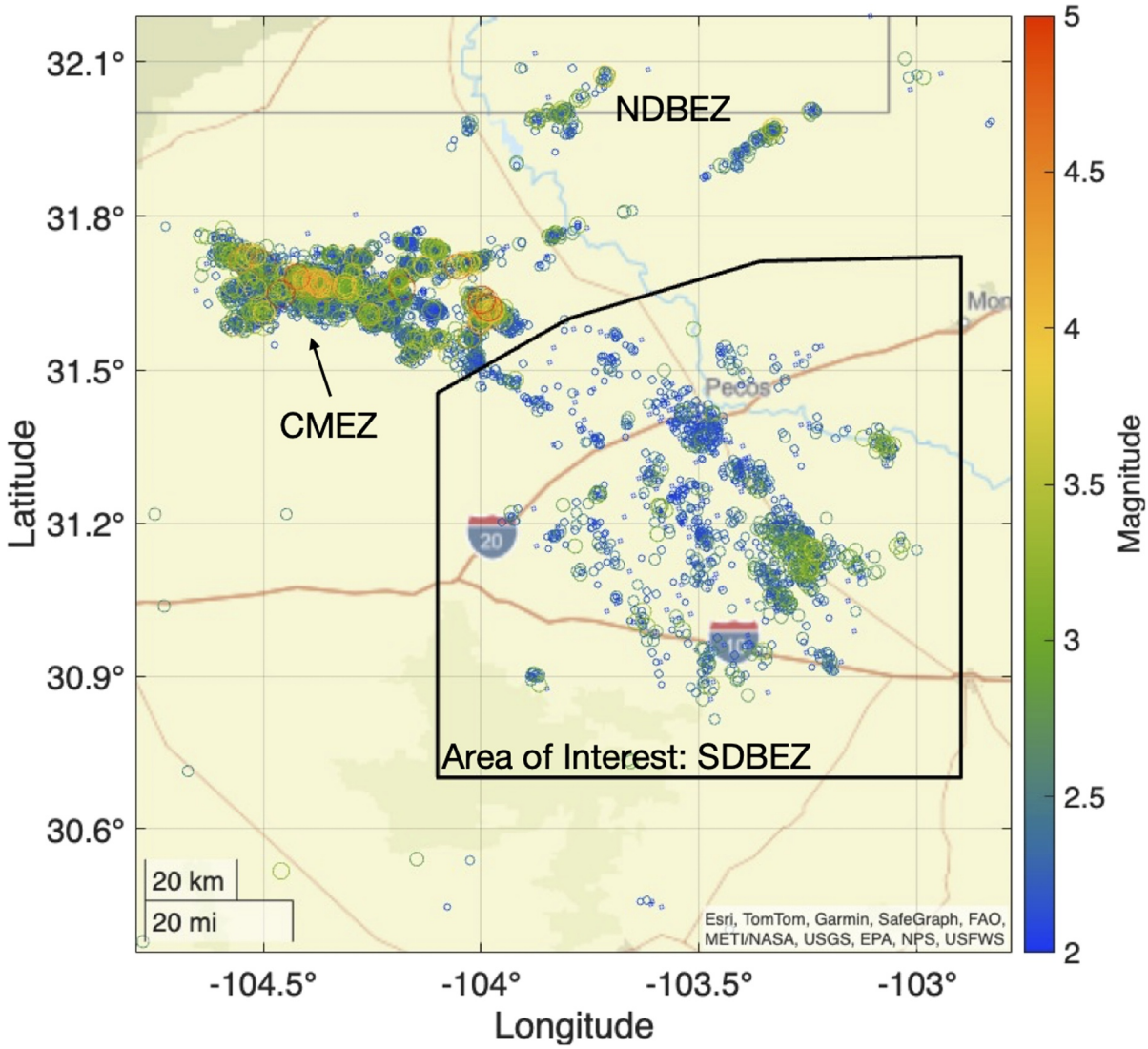

Figure 1. Earthquake catalog used in this study. Circles show earthquakes, sized and colored by magnitude. The black polygon delineates our area of interest, the SDBEZ, excluding the earthquakes in the CMEZ and NDBEZ.

2. Evidence for M_{max} Truncation in Southern Delaware Basin

2.1. Earthquake Catalog

Hennings and Smye (2024) define an induced seismicity "system" as "earthquakes induced by a specific set of anthropogenic agents that interact uniquely with specific geologic elements in an understandable spatial and temporal context." Smye et al. (2024) divide induced seismicity in the Delaware Basin into several distinct systems (Figure 1): the southern Delaware Basin earthquake zone, SDBEZ; the Culberson-Mentone earthquake zone, CMEZ; and the northern Delaware Basin earthquake zone, NDBEZ.

Seismicity in the CMEZ and NDBEZ is primarily caused by WWD into the deep Ellenburger Formation and other Lower Paleozoic strata, situated just above the Precambrian crystalline basement, in some places reaching depths of over 5 km (Smye et al., 2024). In contrast, seismicity in the SDBEZ is primarily caused by WWD into the shallower Delaware Mountain Group, typically at depths of between 1,000 and 2,000 m. Some events in the SDBEZ may also be associated with hydraulic fracturing (Grigoratos et al., 2022), which primarily takes place in the Wolfcamp and Bone Spring Formations, which lie between the shallower Delaware Mountain Group and the underlying Ellenburger Formation. Earthquakes in the NDBEZ and CMEZ occur on deep faults that extend from

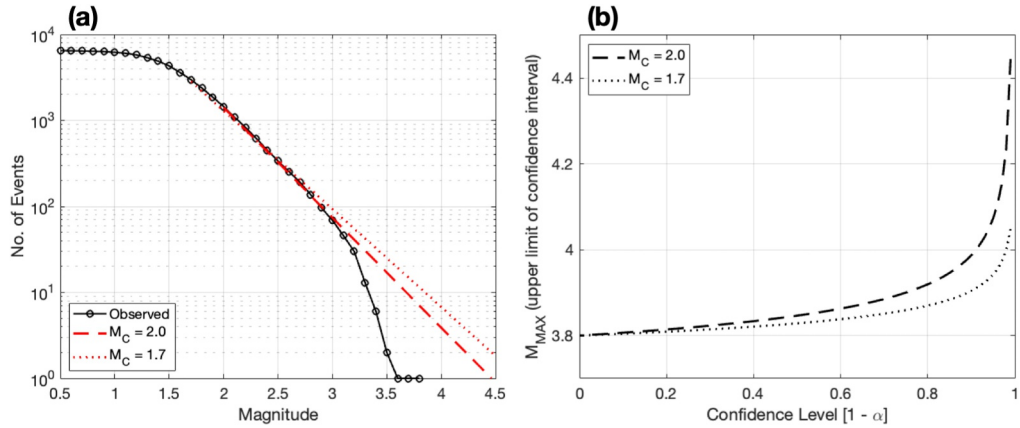

Figure 2. In (a) we show the magnitude frequency distribution for events in the SDBEZ. The red dashed and dotted lines show the G-R distribution fitted with an M_C of 2.0 and 1.7, respectively. In (b) we show the upper limit to the M_{MAX} confidence interval calculated using the method of Holschneider et al. (2011). The dashed and dotted lines show the results when $M_C = 2.0$ and $M_C = 1.7$, respectively.

the Lower Paleozoic injection targets into the underlying basement. In contrast, earthquakes in the SDBEZ occur on shallower faults within the sedimentary section (Hennings et al., 2021; Horne et al., 2022). For representations of the earthquake positions in the SDBEZ area relative to stratigraphy and mapped faults, see for example, Figure 2 of Zoback and Hennings (2025) and Figure 4 of Aziz Zanjani et al. (2025). Previous studies have generally agreed that the SDBEZ seismicity represents triggered rather than driven seismicity (e.g., Huang et al., 2022; Zoback & Hennings, 2025).

Our earthquake data is drawn from the TexNet catalog (Savvaidis et al., 2019), and we use the local magnitudes defined therein. We use all events from 2017 until May 2025. Following the induced seismicity systems defined by Smye et al. (2024), we define an area of interest covering the SDBEZ, but excluding events in the CMEZ and NDBEZ systems, which are caused by deeper WWD activities (Figure 1). The CMEZ and NDBEZ systems do not yet show any evidence of having reached an upper limit magnitude truncation.

2.2. Magnitude Frequency Distribution

The magnitude frequency distribution for the events within the SDBEZ is plotted in Figure 2a. The largest event within the SDBEZ area has a magnitude of M_L 3.8. We use the Aki (1965) method to fit the G-R relationship to the observed magnitudes. We used two methods to independently determine the minimum magnitude of completeness, M_C: the Weimer and Wyss (2000) criterion with a threshold of 95%, and a Kolmogorov-Smirnov test with a 20% significance threshold (following Clauset et al., 2009). Both of these methods gave $M_C = 2.0$, with a corresponding b-value of $b = 1.28$. The reported magnitude of completeness for the TexNet catalog is $M_C = 1.5$ (Savvaidis et al., 2019). A visual inspection of the magnitude frequency distribution shown in Figure 2a suggests that M_C values as low as $M_C = 1.7$ may be reasonable, and to explore the impact of this parameter choice we also compute results with this M_C, which gives a corresponding b-value of $b = 1.14$.

The departure in the observed catalog from the G-R distribution at high magnitudes is immediately apparent in Figure 2a, with larger events being underrepresented in the observed data.

2.3. Determining M_{MAX}

Various methods have been proposed to investigate whether observed earthquake populations have an upper limit truncation, and if so, the magnitude at which they are truncated. In this study we adopt the methods of Holschneider et al. (2011) and Schultz (2024), both of which have recently been applied to other cases of induced seismicity (Schultz et al., 2025).

From Holschneider et al. (2011), the upper interval for M_{MAX} is given by:

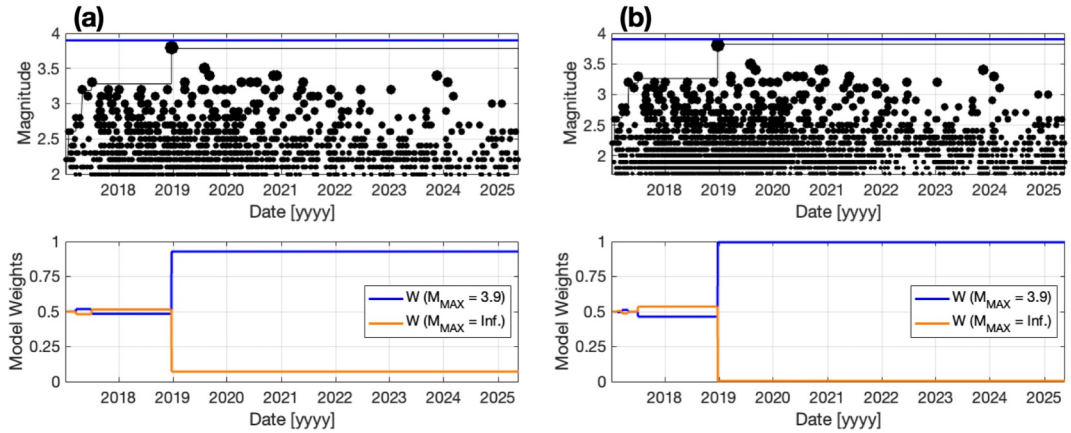

Figure 3. Results of the Schultz (2024) hypothesis testing. The upper panels show the observed seismicity as a function of time (black dots), along with the hypothesized M_{MAX} for the bounded case (blue line). The lower panels show the hypotheses weights for the bounded (blue) and unbounded (orange hypotheses). In (a) we show the results when $M_C = 2.0$, and in (b) we show the results when $M_C = 1.7$.

$$M_{\mathrm{MAX}} = M_C - \frac{1}{\beta}\log_{10}\left[\frac{\exp\left(-\beta\left(M^O_{\mathrm{MAX}} - M_C\right)\right) - 1}{\alpha^{1/n}}\right], \tag{2}$$

where $M^O{}_{\mathrm{MAX}}$ is the largest observed event in the catalog, $\beta = b\ \ln(10)$ is the re-scaled G-R b-value, n is the number of events in the catalog (above the minimum magnitude of completeness), and 1—α is the level of confidence in the M_{MAX} estimate.

The results of this formulation applied to the SDBEZ earthquake catalog are shown in Figure 2b. We show results using $M_C = 2.0$ and $M_C = 1.7$ (and the b-values corresponding thereto). Both results give relatively strong confidence that the observed catalog is truncated at an upper limit M_{MAX} value, and that this upper limit is not significantly higher than M 4.0. At the 95% confidence level, when $M_C = 2.0$, $M_{\mathrm{MAX}} = 4.07$, and when $M_C = 1.7$, $M_{MAX} = 3.94$.

We also use the methods developed by Schultz (2024) to further test whether the SDBEZ magnitudes are constrained by an upper limit truncation. Schultz (2024) examines the distribution of magnitudes against magnitude jumps—the increase in magnitudes between each next largest event within a sequence, $\Delta M^O{}_{\mathrm{MAX}}$—and develops a maximum likelihood estimator for M_{MAX}. This method is based on the concept that, when magnitudes are drawn sequentially from an unbounded G-R distribution, the distributions of magnitudes and magnitude jumps will be the same. When observations are drawn from an upper limit-truncated distribution, the distributions will not be the same, since, as magnitudes approach M_{MAX}, larger jumps to new magnitudes will no longer be possible.

Schultz (2024) showed that this test was better able to discern the influence of an upper limit M_{MAX} truncation on a population of earthquakes. Applying the Schultz (2024) maximum likelihood estimation produces $M_{\mathrm{MAX}} = 3.85$, a value that is only very slightly larger than the largest observed event in the sequence.

Schultz (2024) developed a hypothesis-testing framework to discern between competing models for M_{MAX}. This method uses the Akaike Information Criterion and the Bayesian Information Criterion to compare the log-likelihood ratios between different upper-limit truncations (or the absence thereof).

We assign two alternative hypotheses for M_{MAX}, the first being that an upper limit truncation exists at $M_{\mathrm{MAX}} = 3.9$. The second is that no upper limit truncation exists, and M_{MAX} is infinite. Figure 3 shows the resulting hypothesis weightings produced by the Schultz (2024) method, for our higher and lower choices of M_C. During the first two years of the catalog (2017–2018), the relative weights between two M_{MAX} hypotheses are roughly equal. This result is produced because the numbers of events, and hence the largest observed magnitudes, are significantly below the proposed M_{MAX}. The hypothesis testing is therefore unable to discriminate between a hypothesis that M_{MAX} is infinite and a hypothesis that M_{MAX} is significantly higher than the largest observed events. Once the largest observed magnitude reaches M_{L} 3.8, close to the hypothesized

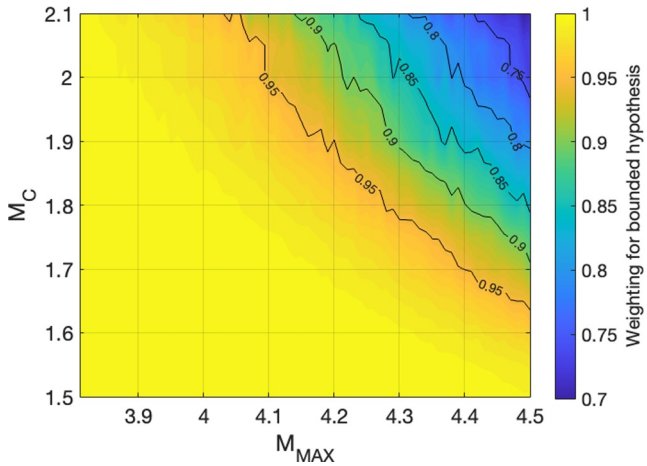

Figure 4. Weighting for the hypothesis that the sequence is bounded by a maximum magnitude, when compared against the alternative hypothesis that no bound is present, as a function of the choice of M_C and hypothesized M_{MAX}.

M_{MAX} value, then the relative weights diverge, with the truncated distribution being strongly favored over the unbounded distribution.

To further explore the sensitivity of the Schultz (2024) hypothesis testing, we compute weightings as a function of M_C and the bounding M_{MAX} value. In doing so, our alternative hypothesis is always that the magnitudes are unbounded. Our point of comparison is at the end of the catalog (i.e., May 2025), where we extract the weighting for the bounded distribution hypothesis. Our results are shown in Figure 4. We find that the bounded hypothesis is strongly favored (weightings are close to 1.0) regardless of the choice of M_C. At high values of M_{MAX} the weightings become lower. This is because, if the M_{MAX} value is significantly larger than the observed magnitudes, then it is not possible to distinguish between an unbounded model and a bounded model where the bound is significantly larger than the observations (Holschneider et al., 2011).

In summary, the magnitudes of earthquakes in the SDBEZ show strong evidence of being truncated at a maximum magnitude of approximately $M_{MAX} \approx 4.0$. In the following section, we explore potential geomechanical factors that could influence the maximum size of induced earthquakes in this system, and discuss the implications for induced seismicity risk management in the SDBEZ, and more generally.

3. Geomechanical Controls on M_{MAX}

The McGarr (2014) volume-based M_{MAX} is often proposed as a limit to injection-induced seismicity magnitudes, though the assumptions on which this method is built are only valid for cases of driven seismicity (McGarr & Majer, 2023). In this formulation, the maximum size of an earthquake is limited by the injected volume, ΔV:

$$M_{MAX} = \frac{2}{3}\log_{10} \mu \Delta V - 6.07, \quad (3)$$

where μ is the shear modulus. Within the SDBEZ, WWD wells have injected more than 1×10^9 m^3 of water. Assuming an arbitrary value for μ of 5 GPa, the McGarr (2014) equation produces $M_{MAX} = 6.4$. Clearly, the overall volume of WWD does not represent a limiting factor for M_{MAX} in the SDBEZ.

Langenbruch et al. (2024) proposed a model where M_{MAX} is controlled by the length of time since injection onset. In this model, the dimensions of the perturbed volume control M_{MAX}, and it is the length of time from injection onset that controls, via diffusion, this size. Langenbruch et al. (2024) model is derived for a single injection point source: where multiple injectors are present, a larger M_{MAX} might be expected if pressure perturbations overlap, creating a larger combined perturbation. Moreover, shallow WWD in the SDBEZ has been ongoing for more than a decade, having increased substantially since 2014. From Table 1 of Langenbruch et al. (2024), M_{MAX} based on injection duration is expected to be greater than M 5.0, and potentially larger than M 6.0. Thus, the duration over which WWD has taken place does not appear to represent a limiting factor for M_{MAX} in the SDBEZ.

The maximum dimensions of faults available to rupture are often invoked as an important control on M_{MAX} (e.g., Wyss, 1979). The relationship between maximum possible fault rupture area, A, and M_{MAX} is given by (Kanamori & Brodsky, 2004):

$$M_{MAX} = \frac{2}{3}\log_{10} \Delta\sigma A^{3/2} - 6.07, \quad (4)$$

where $\Delta\sigma$ is the stress drop, which typically ranges from 0.01 to 100 MPa (Abercrombie & Leary, 1993). Horne et al. (2022) mapped shallow faults in the SDBEZ using 3D reflection seismic surveys. Their mean fault lengths were typically 2–6 km, and their maximum fault lengths were 10–20 km. Their mean fault areas were between 2 and 12 km^2, and maximum surface areas were between 20 and 30 km^2. Clearly, if such faults were capable of

rupturing across their entire area in a single event then earthquakes with magnitudes significantly larger than our observed M_{MAX} would be possible.

However, the shallow faults in the SDBEZ on which the induced seismicity occurs are "strata-bound" (Zoback & Hennings, 2025), that is, they are structurally decoupled from the underlying basement-rooted faults. Seismic reflection imaging of these faults suggests that they have down-dip widths of ~1 km at most (Horne et al., 2022). Likewise, inversion of geodetic observations for events in the SDBEZ have also shown that ruptures are shallow and of limited width (Lee et al., 2023; Pepin et al., 2022). Note that we use the term "width" here to be consistent with previous literature—given the geometry of these faults, this dimension might be better thought of as a fault height. The control exerted by fault width on the maximum possible rupture dimensions has been long debated (e.g., Henry & Das, 2001; Leonard, 2010; Ruff & Kanamori, 1983), primarily focussed on large subduction zone earthquakes where the rupture width is constrained by the thickness of the seismogenic crust.

Key to this debate is the question as to whether earthquakes can rupture the entire along-strike length if a fault has a limited seismogenic width? Where a fault's length is significantly longer than its width, ruptures with large aspect ratios (length/width) would be required to rupture the entire fault plane. However, observational compilations (e.g., Thingbaijam et al., 2017) suggest that small and moderate magnitude earthquakes tend to have aspect ratios close to 1. Dip-slip earthquakes in particular are not typically observed to produce large aspect ratios (Stock & Smith, 2000) and most earthquakes in the SDBEZ are observed to have normal fault focal mechanisms (Huang et al., 2022).

Numerical models have shown that high aspect ratio ruptures require a minimum fault width to occur. As a rupture saturates the up- and down-dip limits of a fault, the release of strain energy becomes constrained, such that it falls below the fracture energy needed to propagate the rupture. Ruptures therefore cannot be sustained and become self-arresting (Weng & Yang, 2017). Weng and Yang (2017) estimated the minimum critical width at which a transition from arrested ruptures (with aspect ratios close to 1) to "breakaway" ruptures (with larger aspect ratios) can occur, finding a minimum value of 8 km. Below this width, rupture aspect ratios cannot increase significantly above 1. Weng and Yang's (2017) model results are consistent with observational compilations, where ruptures with down-dip widths below 8 km have aspect ratios close to 1.

The down-dip widths of the shallow strata-bound faults in the SDBEZ are significantly less than the critical width proposed by Weng and Yang (2017). We recognize that the models presented by Weng and Yang (2017) are generic in nature, and rupture simulations based on the specific geology and geomaterials present in the SDBEZ would be worthwhile. Nevertheless, since the down-dip widths of the shallow faults in the SDBEZ are limited to approximately 1 km, and from Weng and Yang (2017) we expect to have arrested ruptures with aspect ratios close to 1, then the maximum expected rupture area is close to 1 km^2. The corresponding maximum magnitude, assuming $\Delta\sigma = 1$ MPa, is $M_{MAX} = 3.9$. This value closely matches the M_{MAX} values derived from our analysis of the observed magnitude distribution, as described in Section 2.

4. Implications for Management of Induced Seismicity Risk

4.1. Induced Seismicity Hazard in the SDBEZ

The most immediate significance of our finding that the magnitudes of earthquakes in the SDBEZ are truncated by an upper limit maximum magnitude of approximately M 4.0 is on induced seismicity risk assessments for the area, since the implication is that larger earthquakes, such as the $M > 5.0$ events seen in the CMEZ to the north, should not be expected in the SDBEZ regardless of how many smaller magnitude events occur.

However, care should be taken if this value is to be incorporated into future hazard assessments. Our geomechanical interpretation implies that this M_{MAX} bound will only apply to earthquakes occurring on the shallow strata-bound faults within the Delaware Mountain Group. If perturbations from the shallow WWD activities are able to reach and reactivate basement-rooted faults in the underlying strata, then larger events may be possible. We note that for induced seismicity at Groningen, an example of driven seismicity with evidence for a rather low M_{MAX} bound, some induced seismicity hazard assessments included, as a branch with an M_{MAX} logic tree, the possibility that deformation could engage and trigger deeper, larger faults, producing event magnitudes that are larger than M_{MAX} estimates derived from the observed catalog to date (Coppersmith et al., 2022), although the validity of this approach is disputed (Bommer et al., 2024). Also, if WWD into deeper formations, such as the

Ellenburger Formation, were to take place, then larger, basement-rooted faults could be activated, and the geomechanically constrained M_{MAX} would not apply.

4.2. Implications for Induced Seismicity Hazard Management

We have found that, for the SDBEZ, M_{MAX} appears to be constrained not by the lengths of existing faults but by their down-dip widths. This has important implications for site characterization efforts, where a common step in induced seismicity hazard assessment strategies is to map faults and use their lengths to determine expected maximum earthquake magnitudes (e.g., Baisch et al., 2016; Zhou et al., 2024). Our observations suggest that equal or greater focus should be made on characterizing the widths of faults near to candidate industrial sites. Determining fault width can be challenging for faults that extend a significant distance through the sedimentary column (and even into basement strata), since detailed geophysical observations across a broad range of depths will be required, rather than geophysical imaging and characterization that is focused solely or primarily on the depth of the proposed industrial activity.

5. Conclusions

The WWD-induced seismicity in the SDBEZ shows evidence of an upper limit magnitude truncation at a magnitude of $M_{MAX} \approx 4.0$. This is the first observation of such a truncation for a widespread induced seismicity system where events are triggered, rather than industrially driven. The most likely explanation for the truncation is the limited width of the faults within the Delaware Mountain Group. Although some of these faults have lengths of over 10 km along-strike, their down-dip width is limited to approximately 1 km. From rupture mechanics, we anticipate that for faults with limited width, rupture aspect ratios will be close to 1. The corresponding maximum possible rupture dimensions match the observed truncation, giving a plausible geomechanical explanation for this observation. This truncation has significant implications for induced seismicity risk management in the area, although care should be taken since it only applies to events occurring on the shallow, strata-bound faults—if perturbations were transferred downwards to deeper faults then larger events could occur. Our findings imply that constraining down-dip fault widths may be more important than fault lengths when characterizing induced seismicity hazard.

Conflict of Interest

JPV leads the Bristol and Oxford Passive Seismic (BOPS) project. BOPS is funded by a range of operating and oilfield service companies. JPV has also acted and continues to act as an independent consultant for a variety of organisations including hydrocarbon operating companies and governmental organisations on issues pertaining to induced seismicity. None of these organisations had any input into the conception, development or analyses presented in this study.

Data Availability Statement

The seismic catalog data was drawn from the TexNet earthquake catalog at https://catalog.texnet.beg.utexas.edu (last accessed 21/05/2025). The code used to perform the Schultz (2024) tests are available for download at: https://github.com/RyanJamesSchultz/NLE (last accessed 20/01/2026). The same resources are also available online at Zenodo (Schultz, 2025).

Acknowledgments
JPV received funding to support this study from the UK Natural Environment Research Council SeisGreen Grant (Grant NE/W009293/1). RS is supported by the Swiss National Science Foundation, under project Grant TMPFP2_224393. We would like to thank Dr Cornelius Langenbruch and Prof. Mark Zoback for their constructive reviews of our manuscript.

References

Abercrombie, R., & Leary, P. (1993). Source parameters of small earthquakes recorded at 2.5 km depth, Cajon Pass, southern California: Implications for earthquake scaling. *Geophysical Research Letters*, *20*(14), 1511–1514. https://doi.org/10.1029/93gl00367

Aki, K. (1965). Maximum likelihood estimate of b in the formula log N = a−bM and its confidence limits. *Bulletin of the Earthquake Research Institute Tokyo University*, *43*, 237–239.

Aziz Zanjani, A., DeShon, H. R., Karanam, V., & Savvaidis, A. (2025). Insights into spatiotemporal evolution of induced earthquakes in the southern Delaware Basin using calibrated relocations from the TexNet catalog (2017–2022). *Earth and Space Science*, *12*(6), e2024EA004027. https://doi.org/10.1029/2024ea004027

Baisch, S., Koch, C., Stang, H., Pittens, B., Drijver, B., & Buik, N. (2016). Defining the framework for seismic hazard assessment in geothermal projects V0.1: Technical report for the Ministry of economic affairs. Retrieved from https://www.geothermie.nl/images/Onderzoeken-en-rapporten/01_10_16_Framework_Seismiciteit/Kennisagenda_-_Defining_framework_for_Seismic_Hazard_Assessment_in_Geothermal_Projects_-_Technical_Report_-_161005.pdf

Boitz, N., Langenbruch, C., & Shapiro, S. A. (2024). Production-induced seismicity indicates a low risk of strong earthquakes in the Groningen gas field. *Nature Communications*, *15*(1), 329. https://doi.org/10.1038/s41467-023-44485-4

Bommer, J. J., van Elk, J., & Zoback, M. D. (2024). Estimating the maximum magnitude of induced earthquakes in the Groningen gas field, the Netherlands. *Bulletin of the Seismological Society of America*, *114*(6), 2804–2822. https://doi.org/10.1785/0120240054

Bommer, J. J., & Verdon, J. P. (2024). The maximum magnitude of natural and induced earthquakes. *Geomechanics and Geophysics for Geo-Energy and Geo-Resources*, *10*(1), 172. https://doi.org/10.1007/s40948-024-00895-2

Clarke, H., Verdon, J. P., Kettlety, T., Baird, A. F., & Kendall, J.-M. (2019). Real time imaging, forecasting and management of human-induced seismicity at Preston New Road, Lancashire. *Seismological Research Letters*, *90*, 1902–1915. https://doi.org/10.1785/0220190110

Clauset, A., Shalizi, C. R., & Newman, M. E. J. (2009). Power-law distributions in empirical data: Society of industrial and. *Applied Mathematics Reviews*, *51*(4), 661–703. https://doi.org/10.1137/070710111

Coppersmith, K., Ake, J., Bungum, H., Dahm, T., Main, I., McGarr, A., et al. (2022). *Second report from the expert panel on maximum magnitude estimates for probabilistic seismic hazard and risk modelling in Groningen gas field*. Nederlandse Aardolie Maatschappij. Retrieved from https://nam-onderzoeksrapporten.data-app.nl/reports/download/groningen/en/77951661-552a-46bc-9f2e-f1580cd6abc3

Galis, M., Ampuero, J. P., Mai, P. M., & Cappa, F. (2017). Induced seismicity provides insight into why earthquake ruptures stop. *Science Advances*, *3*(12), eaap7528. https://doi.org/10.1126/sciadv.aap7528

Grigoratos, I., Savvaidis, A., & Rathje, E. (2022). Distinguishing the causal factors of induced seismicity in the Delaware basin: Hydraulic fracturing or wastewater disposal. *Seismological Research Letters*, *93*(5), 2640–2658. https://doi.org/10.1785/0220210320

Gutenberg, B., & Richter, C. (1944). Frequency of earthquakes in California. *Bulletin of the Seismological Society of America*, *34*(4), 591–610. https://doi.org/10.1785/bssa0340040185

Hallo, M., Oprsal, I., Eisner, L., & Ali, M. Y. (2014). Prediction of magnitude of the largest potentially induced seismic event. *Journal of Seismology*, *18*(3), 421–431. https://doi.org/10.1007/s10950-014-9417-4

Hennings, P., Dvory, N., Horne, E., Li, P., Savvaidis, A., & Zoback, M. (2021). Stability of the fault systems that host induced earthquakes in the Delaware Basin of west Texas and southeast New Mexico. *The Seismic Record*, *1*(2), 96–106. https://doi.org/10.1785/0320210020

Hennings, P., & Smye, K. (2024). Knowns, questions, and implications of induced seismicity in the Permian Basin, USA. *American Association of Petroleum Geologists Bulletin*, *108*(12), 2201–2214. https://doi.org/10.1306/08292424051

Henry, C., & Das, S. (2001). Aftershock zones of large shallow earthquakes: Fault dimensions, aftershock area expansion and scaling relations. *Geophysical Journal International*, *147*(2), 272–293. https://doi.org/10.1046/j.1365-246x.2001.00522.x

Hill, R. G., Weingarten, M., Langenbruch, C., & Fialko, Y. (2024). Mitigation and optimization of induced seismicity using physics-based forecasting. *Journal of Geophysical Research*, *129*(11), e2024JB028759. https://doi.org/10.1029/2024jb028759

Holschneider, M., Zöller, G., & Hainzl, S. (2011). Estimation of the maximum possible magnitude in the framework of a doubly truncated Gutenberg-Richter model. *Bulletin of the Seismological Society of America*, *101*(4), 1649–1659. https://doi.org/10.1785/0120100289

Horne, E. A., Hennings, P. H., Smye, K. M., Staniewicz, S., Chen, J., & Savvaidis, A. (2022). Structural characteristics of shallow faults in the Delaware Basin. *Interpretation*, *10*(4), T807–T835. https://doi.org/10.1190/int-2022-0005.1

Huang, G. D., Horne, E., Kavoura, F., & Savvaidis, A. (2022). Characteristics of seismogenic structures and 3D stress state of the Delaware Basin of west Texas as constrained by earthquake source mechanisms. *Seismological Research Letters*, *93*(6), 3363–3372. https://doi.org/10.1785/0220220054

Kanamori, H., & Brodsky, E. E. (2004). The physics of earthquakes. *Reports on Progress in Physics*, *67*(8), 1429–1496. https://doi.org/10.1088/0034-4885/67/8/r03

Kettlety, T., Verdon, J. P., Butcher, A., Hampson, M., & Craddock, L. (2021). High-resolution imaging of the M_L 2.9 August 2019 earthquake in Lancashire, United Kingdom, induced by hydraulic fracturing during Preston New Road PNR-2 operations. *Seismological Research Letters*, *92*(1), 151–169. https://doi.org/10.1785/0220200187

Kwiatek, G., Saamo, T., Ader, T., Bluemle, F., Bohnhoff, M., Chendorain, M., et al. (2019). Controlling fluid-induced seismicity during a 6.1-km-deep geothermal stimulation in Finland. *Science Advances*, *5*, eaav7224. https://doi.org/10.1126/sciadv.aav7224

Langenbruch, C., Moein, M. J. A., & Shapiro, S. A. (2024). Are maximum magnitudes of induced earthquakes controlled by pressure diffusion. *Philosophical Transactions of the Royal Society A*, *382*(2276), 20230184. https://doi.org/10.1098/rsta.2023.0184

Langenbruch, C., & Zoback, M. D. (2016). How will induced seismicity in Oklahoma respond to decreased saltwater injection rates. *Science Advances*, *2*(11), e1601542. https://doi.org/10.1126/sciadv.1601542

Lee, H. P., Staniewicz, S., Chen, J., Hennings, P., & Olson, J. E. (2023). Subsurface deformation monitoring with InSAR and elastic inversion modeling in west Texas. *Geoenergy Science and Engineering*, *231*, 212299. https://doi.org/10.1016/j.geoen.2023.212299

Leonard, M. (2010). Earthquake fault scaling: Self-consistent relating of rupture length, width, average displacement, and moment release. *Bulletin of the Seismological Society of America*, *100*(5A), 1971–1988. https://doi.org/10.1785/0120090189

McGarr, A. (1976). Seismic moments and volume changes. *Journal of Geophysical Research*, *81*(8), 1487–1494. https://doi.org/10.1029/jb081i008p01487

McGarr, A. (2014). Maximum magnitude earthquakes induced by fluid injection. *Journal of Geophysical Research*, *119*(2), 1008–1019. https://doi.org/10.1002/2013jb010597

McGarr, A., & Majer, E. L. (2023). The 2017 Pohang, South Korea, Mw 5.4 main shock was either natural or triggered, but not induced. *Geothermics*, *107*, 102612. https://doi.org/10.1016/j.geothermics.2022.102612

McNamara, D. E., Benz, H. M., Herrmann, R. B., Bergman, E. A., Earle, P., Holland, A., et al. (2015). Earthquake hypocenters and focal mechanisms in central Oklahoma reveal a complex system of reactivated subsurface strike-slip faulting. *Geophysical Research Letters*, *42*(8), 2742–2749. https://doi.org/10.1002/2014gl062730

Pepin, K. S., Ellsworth, W. L., Sheng, Y., & Zebker, H. A. (2022). Shallow aseismic slip in the Delaware Basin determined by Sentinel-1 InSAR. *Journal of Geophysical Research*, *127*(2), e2021JB023157. https://doi.org/10.1029/2021jb023157

Rodríguez-Pradilla, G., Eaton, D. W., & Verdon, J. P. (2022). Basin-scale multi-decadal analysis of hydraulic fracturing and seismicity in western Canada shows non-recurrence of induced runaway fault-rupture. *Scientific Reports*, *12*, 14463.

Ruff, L., & Kanamori, H. (1983). Seismic coupling and uncoupling at subduction zones. *Tectonophysics*, *99*(2–4), 99–117. https://doi.org/10.1016/0040-1951(83)90097-5

Savvaidis, A., Young, B., Huang, G. D., & Lomax, A. (2019). TexNet: A statewide seismological network. *Seismological Research Letters*, *90*, 1702–1715. https://doi.org/10.1785/0220180350

Schultz, R. (2024). Inferring maximum magnitudes from the ordered sequence of large earthquakes. *Philosophical Transactions of the Royal Society A*, *382*(2276), 20230185. https://doi.org/10.1098/rsta.2023.0185

Schultz, R. (2025). RyanJamesSchultz/NLE: v1 (version v1) [Software]. *Zenodo*. https://doi.org/10.5281/zenodo.17140995

Schultz, R., Lanza, F., Dyer, B., Karvounis, D., Fiori, R., Shi, P., et al. (2025). The bound growth of induced earthquakes could de-risk hydraulic fracturing. *Nature Communications*, *6*(1), 995. https://doi.org/10.1038/s43247-025-02881-2

Segall, P. (1989). Earthquakes triggered by fluid extraction. *Geology*, *17*(10), 942–946. https://doi.org/10.1130/0091-7613(1989)017<0942:etbfe>2.3.co;2

Shapiro, S. A., Dinske, C., Langenbruch, C., & Wenzel, F. (2010). Seismogenic index and magnitude probability of earthquakes induced during reservoir fluid stimulations. *The Leading Edge*, *29*(3), 304–308. https://doi.org/10.1190/1.3353727

Shapiro, S. A., Krüger, O. S., Dinske, C., & Langenbruch, C. (2011). Magnitudes of induced earthquakes and geometric scales of fluid-stimulated rock volumes. *Geophysics*, *76*(6), WC55–WC63. https://doi.org/10.1190/geo2010-0349.1

Smye, K. M., Ge, J., Calle, A., Morris, A., Horne, E. A., Eastwood, R. L., et al. (2024). Role of deep fluid injection in induced seismicity in the Delaware Basin, West Texas and southeast New Mexico. *Geochemistry, Geophysics, Geosystems*, *25*(6), e2023GC011260. https://doi.org/10.1029/2023gc011260

Stock, C., & Smith, E. G. C. (2000). Evidence for different scaling of earthquake source parameters for large earthquakes depending on faulting mechanism. *Geophysical Journal International*, *143*(1), 157–162. https://doi.org/10.1046/j.1365-246x.2000.00225.x

Thingbaijam, K. K. S., Mai, P. M., & Goda, K. (2017). New empirical earthquake source-scaling laws. *Bulletin of the Seismological Society of America*, *107*(5), 2225–2246. https://doi.org/10.1785/0120170017

van der Elst, N. J., Page, M. T., Weiser, D. A., Goebel, T. H. W., & Hosseini, S. M. (2016). Induced earthquake magnitudes are as large as (statistically) expected. *Journal of Geophysical Research*, *121*(6), 4575–4590. https://doi.org/10.1002/2016jb012818

Verdon, J. P., Kendall, J.-M., Butcher, A., Luckett, R., & Baptie, B. J. (2018). Seismicity induced by longwall coal mining at the Thoresby Colliery, Nottinghamshire, U.K. *Geophysical Journal International*, *212*(2), 942–954. https://doi.org/10.1093/gji/ggx465

Walsh, F. R., & Zoback, M. D. (2016). Probabilistic assessment of potential fault slip related to injection-induced earthquakes: Application to north-central Oklahoma, USA. *Geology*, *44*(12), 991–994. https://doi.org/10.1130/g38275.1

Watkins, T. J. M., Verdon, J. P., & Rodríguez-Pradilla, G. (2023). The temporal evolution of induced seismicity sequences generated by long-term, low pressure fluid injection. *Journal of Seismology*, *27*, 243–259.

Weimer, S., & Wyss, M. (2000). Minimum magnitude of completeness in earthquake catalogs: Examples from Alaska, the western United States, and Japan. *Bulletin of the Seismological Society of America*, *90*, 859–869.

Weng, H., & Yang, H. (2017). Seismogenic width controls aspect ratios of earthquake ruptures. *Geophysical Research Letters*, *44*(6), 2725–2732. https://doi.org/10.1002/2016gl072168

Wyss, M. (1979). Estimating maximum expectable magnitude of earthquakes from fault dimensions. *Geology*, *7*, 336–340. https://doi.org/10.1130/0091-7613(1979)7<336:ememoe>2.0.co;2

Zhou, W., Lanza, F., Grigoratos, I., Schultz, R., Cousse, J., Trutnevyte, E., et al. (2024). Managing induced seismicity risks from enhanced geothermal systems: A good practice guideline. *Reviews of Geophysics*, *62*(4), e2024RG000849. https://doi.org/10.1029/2024rg000849

Zoback, M., & Hennings, P. (2025). Implications of earthquakes triggered by massive injection of produced water in saline aquifers for large-scale geologic storage of CO_2. *International Journal of Greenhouse Gas Control*, *146*, 104447. https://doi.org/10.1016/j.ijggc.2025.104447

Zöller, G., & Holschneider, M. (2016). The maximum possible and the maximum expected earthquake magnitude for production-induced earthquakes at the gas field in Groningen, the Netherlands. *Bulletin of the Seismological Society of America*, *106*, 2917–2921.